Applied Catalysis B: Environmental 176–177 (2015) 62–69

Contents lists available at ScienceDirect

Applied Catalysis B: Environmental

journal homepage: www.elsevier.com/locate/apcatb

Synthesis of flower-like Ag/AgCl-Bi_2MoO_6 plasmonic photocatalysts with enhanced visible-light photocatalytic performance

Xiaoxuan Li [a], Siman Fang [a], Lei Ge [a,b,*], Changcun Han [b], Ping Qiu [b], Weilong Liu [b]

[a] State Key Laboratory of Heavy Oil Processing, College of Science, China University of Petroleum Beijing, No. 18 Fuxue Rd., Beijing 102249, PR China
[b] Department of Materials Science and Engineering, College of Science, China University of Petroleum Beijing, No. 18 Fuxue Rd., Beijing 102249, PR China

ARTICLE INFO

Article history:
Received 30 December 2014
Received in revised form 18 March 2015
Accepted 22 March 2015
Available online 24 March 2015

Keywords:
Flower-like Bi_2MoO_6 spheres
Composite photocatalysts
Photocatalysis
Ag/AgCl

ABSTRACT

A novel plasmonic photocatalysts of Ag/AgCl-Bi_2MoO_6 was successfully synthesized via a simple and mild wet-chemical process. The physical and photophysical properties of the as-prepared Ag/AgCl-Bi_2MoO_6 samples were characterized by X-ray diffraction (XRD), scanning electron microscopy (SEM), transmission electron microscope (TEM), Ultraviolet–visible diffuse reflection spectroscopy (DRS), electron spin resonance (ESR), photoluminescence emission spectra (PL) and surface photovoltage spectroscopy (SPV). The interaction between Ag/AgCl and Bi_2MoO_6 has been investigated by X-ray photoelectron spectroscopy (XPS) analysis, and which is facile to the electron transfer between Ag/AgCl and Bi_2MoO_6 and result in the enhancing photocatalytic activity of Ag/AgCl-Bi_2MoO_6 composite. The photocatalytic experiments indicate that the Ag/AgCl species can efficiently promote the separation efficiency of photo-generated charge carriers in Bi_2MoO_6, and consequently improve the RhB photodegradation activity. The 20 wt% Ag/AgCl-Bi_2MoO_6 sample shows the highest photocatalytic activity, the degradation constant of 20 wt% Ag/AgCl-Bi_2MoO_6 was as high as 4 times to that of pure Bi_2MoO_6. A possible catalytic mechanism for Ag/AgCl-Bi_2MoO_6 is proposed, which can be attributed to the surface plasmon resonance (SPR) effect from Ag/AgCl species.

1. Introduction

Nowadays, water pollution is one of the most serious environmental problems. The increasing water pollution crisis urges people to develop efficient semiconductor photocatalysts by using solar energy in visible light [1–6]. In the various semiconductors, titanium dioxide (TiO_2) is a sufficient available and non-toxic semiconductor; the design and exploration of photocatalysts based on TiO_2 are considered more promising [7–10]. However, because of the large band gap of TiO_2 (3.2 eV), it can only utilize 7% of solar energy (UV range), resulting in low utilization efficiency of solar spectrum.

In recent years, researchers designed several novel photocatalytic materials in order to enhance the visible light activity, such as Bi-based [11–16], Ag-based [11,17], W-containing photocatalysts [18] and so on. Among these visible-light catalysts, Bi_2MoO_6 has been found to show excellent visible-light-driven photocatalytic activity for degradation of organic contaminants [11,15,16,19–21]. However, improving the photocatalytic efficiency of Bi_2MoO_6 to satisfy the practical application is still a challenge due to the poor quantum yield of pure Bi_2MoO_6. To overcome these drawbacks of Bi_2MoO_6 photocatalysts, the design and construction of novel composite photocatalysts have become one of the most effective approaches for improving degradation activity of organics [22–26]. Using semiconductors and/or metals compound with Bi_2MoO_6 can lead to more efficient interfacial charge transfer and enhance the photo-induced charge separation. So far, a variety of Bi_2MoO_6 composites, such as Bi_2MoO_6/TiO_2, Bi_2MoO_6/Ag_3PO_4 have been reported as photocatalysts [15,27]. Recently, Ag/AgX (Cl, Br and I) is widely used to modify the semiconductor photocatalysts [28,16,17,29]. The highly dispersed AgX species can improve the separation efficiency of photo-generated charge carriers, and enhance the photocatalytic activity of the substrates. Furthermore, under visible light irradiation, photogenerated electron–hole pairs are separated on the surface of Ag NPs due to the surface plasmon resonance (SPR) effect [30–32].

Based on the above analysis, it is expected that using Ag/AgCl to modify the Bi_2MoO_6 may effectively improve separation efficiency of electron-hole pairs and catalytic activity. In the present work, a facile approach was developed for the first time to

* Corresponding author at: Department of Materials Science and Engineering, College of Science, China University of Petroleum Beijing, No. 18 Fuxue Rd., Beijing 102249, PR China. Tel.: +86 10 89739096.
E-mail address: gelei08@sina.com (L. Ge).

http://dx.doi.org/10.1016/j.apcatb.2015.03.042
0926-3373/

synthesize the Ag/AgCl-Bi_2MoO_6 photocatalyst with SPR (surface plasmon resonance) effect. The photocatalytic activity of Ag/AgCl-Bi_2MoO_6 samples was investigated by degradation of rhodamine B (RhB) under visible light irradiation. The possible catalytic mechanisms for improved photocatalytic performance were also explored in detail. The outstanding properties associated with the novel Ag/AgCl-Bi_2MoO_6 composite materials suggested that they can be used as a novel light harvesting catalyst for given applications in heterogeneous photocatalysis.

2. Experimental

2.1. Materials

Silver nitrate ($AgNO_3$, Sigma–Aldrich, 99%), sodium chloride (NaCl, 99.5% A.R.), bismuth nitrate pentahydrate ($Bi(NO_3)_3{\cdot}5H_2O$, Aladdin, 98% A.C.S), sodium molybdate dehydrate ($Na_2MoO_4{\cdot}2H_2O$, Aladdin, A.R.), ethyl alcohol (EtOH, A.R.), ethylene glycol (A.R.) and rhodamine B (RhB, AR) were used as received without additional purification or treatment. Milli-Q water was used as the solvent for all of the solutions or dispersions.

2.2. Preparation of flower-like Bi_2MoO_6 spheres

The flower-like Bi_2MoO_6 spheres were prepared according to the following procedure. In a typical process, $Bi(NO_3)_3{\cdot}5H_2O$ (1.6866 g) and $Na_2MoO_4{\cdot}2H_2O$ (0.4210 g) were dissolved separately in ethylene glycol (5 ml) under magnetic stirring. The two solutions were mixed together, then ethanol (20 ml) was added slowly, and the solution was stirred for 10 min. The resulting clear solution was transferred into a 100 ml Teflon-lined stainless steel autoclave, which was heated to 160 °C and maintained at this temperature for 24 h. Subsequently, the autoclave was cooled naturally to room temperature. The obtained samples were filtered, washed with ethanol, dried at 80 °C in air, and calcined at 400 °C for 2 h.

2.3. Preparation of Ag/AgCl-Bi_2MoO_6 composite sample

All deposited samples were synthesized through the deposition and precipitation process. Briefly, Bi_2MoO_6 (0.32 g) were added to distilled water (60 ml) to get solution A, and the suspension was sonicated for 30 min. Then, 0.24 g of NaCl was added into solution A to form solution B. 0.0952 g $AgNO_3$ (mass ratio of AgCl to AgCl/Bi_2MoO_6 was 20%) were added to 20 ml distilled water (named as solution C). Solution C was added drop-wise into solution B with vigorous stirring. The resulting suspension was stirred at room temperature for 30 min. All the above processes were performed in the dark. The products were filtered, washed with distilled water to remove residual ions (Na^+ and Cl^-).

The synthesis process of Ag/AgCl-Bi_2MoO_6 composite was described as follows: 0.3 g AgCl/Bi_2MoO_6 dispersed into 20 ml deionized water solution. Then, Ag nanoparticles were obtained on the surface of AgCl by photo-reduction technique. In the photo-reduction process, the suspension was illuminated by solar simulator 300 W Xe lamp (PLS-SXE300, Beijing Perfect Light Technology Co., Ltd.) for 30 min. All the samples were finally collected after centrifugation, washed with ethanol and deionized water; the final products were dried at 60 °C for 12 h and named as 20 wt% Ag/AgCl-Bi_2MoO_6 (B-4). Similarly, pure Bi_2MoO_6 (B-1), 2 wt% Ag/AgCl-Bi_2MoO_6 (B-2), 10 wt% Ag/AgCl-Bi_2MoO_6 (B-3), 30 wt% Ag/AgCl-Bi_2MoO_6 (B-5) and pure Ag/AgCl (A-1) samples were prepared.

2.4. Characterization

The crystal phase of Bi_2MoO_6, Ag/AgCl and Ag/AgCl-Bi_2MoO_6 powders was analyzed by X-ray diffraction (XRD; Bruker D8 Advance, X-ray diffractometer) with CuKa radiation at a scan rate of 5 min^{-1}, in the 2θ range of 20–70°. The acceleration voltage and the applied current were 40KV and 40 mA, respectively. The morphology of the samples was examined by filed emission scanning electron microscopy (FESEM, FEI Quanta 200F; accelerating voltage = 10KV) and high-resolution transmission electron microscopy (HRTEM, JEM-2100, accelerating voltage 200 kV). UV–vis diffuse reflection spectroscopy (DRS) was performed on a Shimadzu UV-4100 spectrophotometer using $BaSO_4$ as the reference material. The X-ray photoelectron spectroscopy (XPS) was measured in a PHI 5300 ESCA system. The beam voltage was 3.0 eV, and the energy of Ar ion beam was 1.0 keV. The binding energies were normalized to the signal for adventitious carbon at 284.6 eV. The electron spin resonance (ESR) signals of spin-trapped oxidative radicals were obtained on a Bruker model ESR JES-FA200 spectrometer equipped with a quanta-Ray Nd: YAG laser system as the light source with a UV-cutoff filter (λ = 400 nm). The PL spectra of the photocatalysts were detected using a Varian Cary Eclipse spectrometer with excitation wavelength of 395 nm.

2.5. SPV measurements

The surface photovoltage (SPV) measurement was carried out on a surface photovoltage spectroscopy (PL-SPS/IPCE1000 Beijing Perfect Light Technology Co., Ltd.). The measurement system consists of a source of monochromatic light, a lock-in amplifier (SR830, Stanford research systems, Inc.) with a light chopper (SR540, Stanford research systems, Inc.), and a simple chamber. The monochromatic light is provided by passing light from a 500 W xenon lamp (CHFXQ500 W, global xenon lamp power) though a grating monochromator (Omni-5007, No. 09010, Zolix), which chopped with a frequency of 24 Hz. All the measurements were operated at room temperature and under ambient pressure.

2.6. Evaluation of photocatalytic performance

The application of Ag/AgCl-Bi_2MoO_6 nanocomposite for the degradation of organic dye RhB was investigated under visible-light irradiation at room temperature. In a typical procedure, a 50 mg amount photocatalyst powder was suspended in 100 ml RhB solution (10 mg/l). The solution was stirred for 30 min in the dark before the Xe lamp (300 W, PLS-SXE300, Beijing Perfect Light Technology

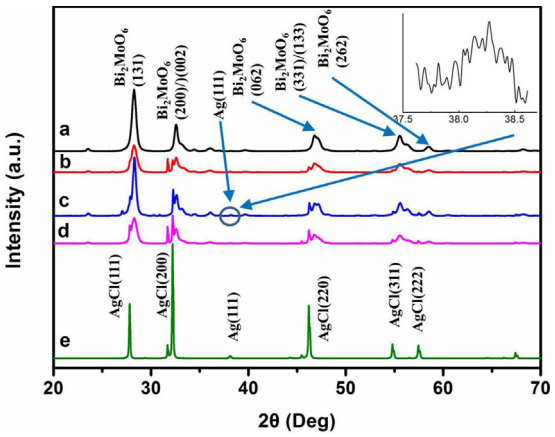

Fig. 1. XRD patterns of as-prepared samples: (a) Bi_2MoO_6, (b) 10 wt% Ag/AgCl-Bi_2MoO_6, (C) 20 wt% Ag/AgCl-Bi_2MoO_6, (d) 30 wt% Ag/AgCl-Bi_2MoO_6 and (e) Ag/AgCl.

Co., Ltd.) coupled with a UV-cutoff filter (400 nm) was turned on to start irradiation to ensure the adsorption/desorption equilibrium between the photocatalysts and the dyes. The light intensity employed was 72 mW cm^{-2}. The solution was sampled in certain intervals and centrifuged, and the above liquid was then monitored by UV-1700 spectrometer at 553 nm. Total organic carbon (TOC) of RhB dye was measured with a Jena multi N/C 2100 TOC analysis system.

In the phenol photodegradation process, a 50 mg amount photocatalyst powder was suspended in 100 ml phenol solution (10 mg/l). Other steps are the same with RhB degradation process. The solution was sampled in certain intervals and centrifuged, and the above liquid was then monitored by UV-1700 spectrometer at 270 nm (quartz cuvette).

3. Results and discussion

3.1. Characterization of Ag/AgCl-Bi_2MoO_6 composite

The X-ray diffraction (XRD) patterns of as-prepared samples are shown in Fig. 1. The pure Bi_2MoO_6 sample (Fig. 1a) shows intense diffraction peaks at $2\theta = 28.1^\circ$, 32.3°, 46.9°, 55.5° and 58.5°, which can be indexed to the Bi_2MoO_6 (1 3 1), (2 0 0)/(0 0 2), (0 6 2), (3 3 1)/(1 3 3) and (2 6 2) planes, respectively (JCPDS No. 76-2388) [16]. The pure Ag/AgCl sample (Fig. 1e) presents diffraction peaks at $2\theta = 27.8^\circ$, 32.2°, 46.2°, 54.8° and 57.5° are attributed to (1 1 1), (2 0 0), (2 2 0), (3 1 1) and (2 2 2) crystal planes of AgCl (JCPDS No. 85-1355) [33]. The results suggest that both AgCl and Bi_2MoO_6

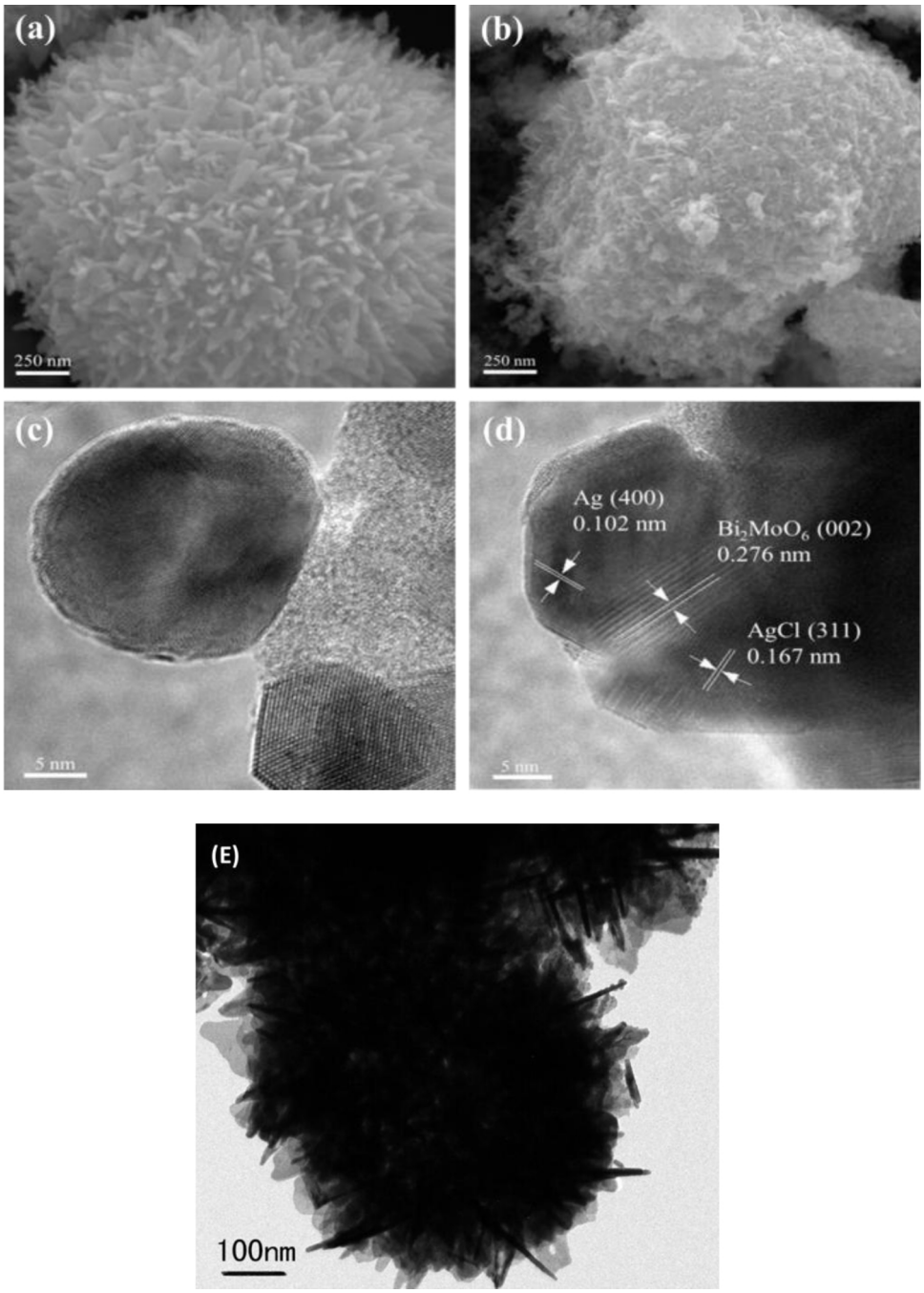

Fig. 2. SEM images of pure Bi_2MoO_6 (a), 20 wt%Ag/AgCl-Bi_2MoO_6 (b) and TEM images of 20 wt%Ag/AgCl-Bi_2MoO_6 (c), (d) and TEM images of pure Bi_2MoO_6 (e).

with a good crystallinity have been formed. As shown in Fig. 1b–e, the weak peaks appear around the scattering angle of $2\theta = 38.1^\circ$ (Fig. 1, inset), which can be ascribed to the metallic Ag (JCPDS No. 87-717) [34]. It is obvious that the diffraction intensity of the AgCl peaks enhance gradually with the increasing Ag/AgCl contents. No characteristic peaks attributing to impurities or other phases are detected, demonstrating that the obtained products are composed of metallic Ag, AgCl and Bi_2MoO_6. Fig. 2 illustrates the SEM and TEM images of Bi_2MoO_6 and 20 wt% Ag/AgCl-Bi_2MoO_6 samples. From the image shown in Fig. 2a, it is easy to observe that the flower-like Bi_2MoO_6 are in fact assembled by a mount of very thin flakes with an average thickness of about 10 nm. Fig. 2e shows that the inner structure of Bi_2MoO_6 is not solid sphere, because the inner is alternating light and dark. With the addition of Ag/AgCl, it is obvious that there are several nanoparticles on the surface of flower-like Bi_2MoO_6 (Fig. 2b). The Ag/AgCl- Bi_2MoO_6 sample was

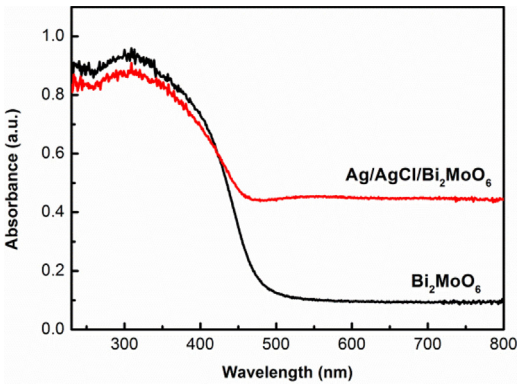

Fig. 3. UV–visible diffuse reflectance spectrum of the samples: (A) Bi_2MoO_6; (B) 20 wt% Ag/AgCl-Bi_2MoO_6.

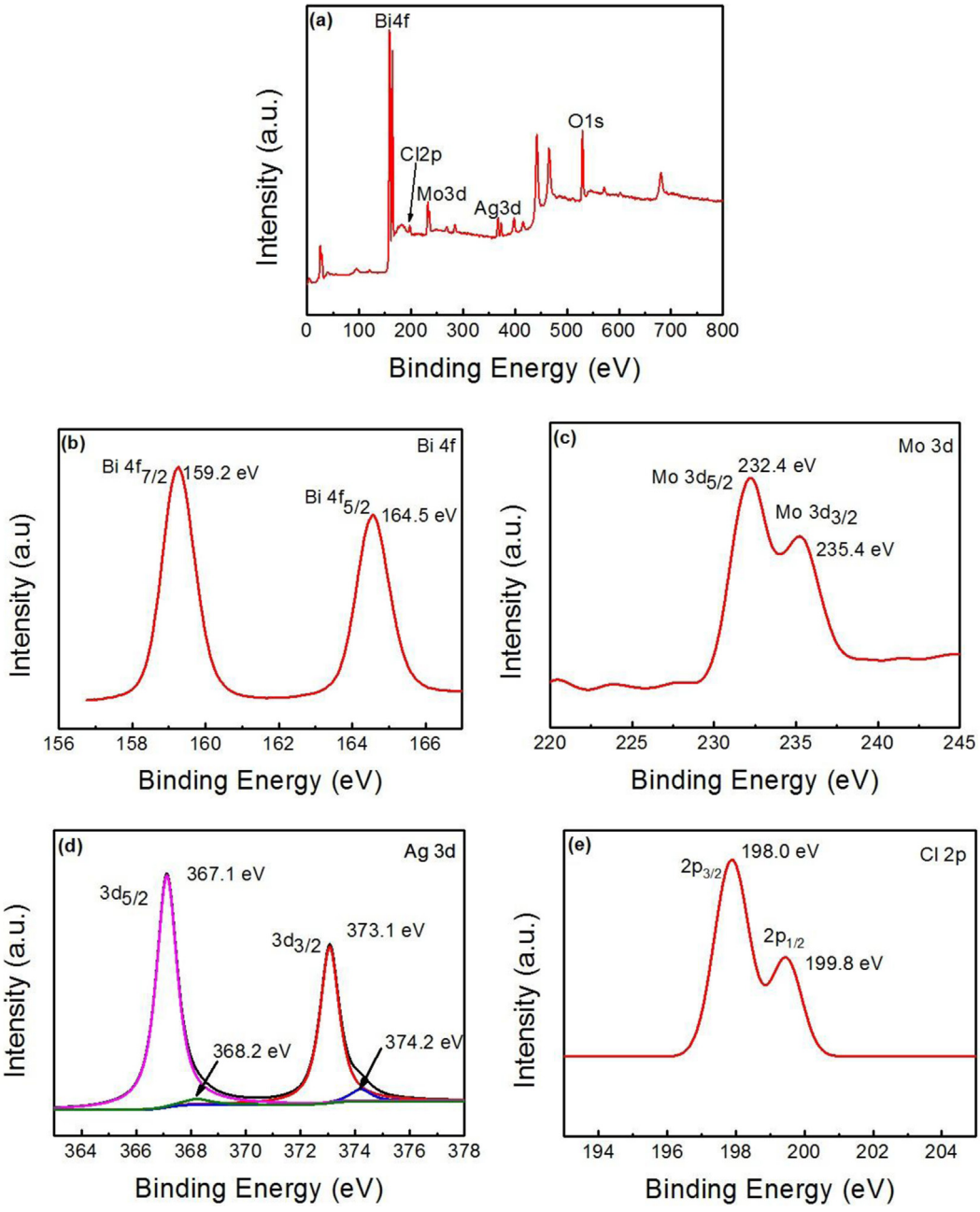

Fig. 4. XPS spectra of the 20 wt% Ag/AgCl-Bi_2MoO_6: (a) the survey spectra, (b) Bi 4f, (c) Mo3d, (d) Ag 3d, (e) Cl 2p.

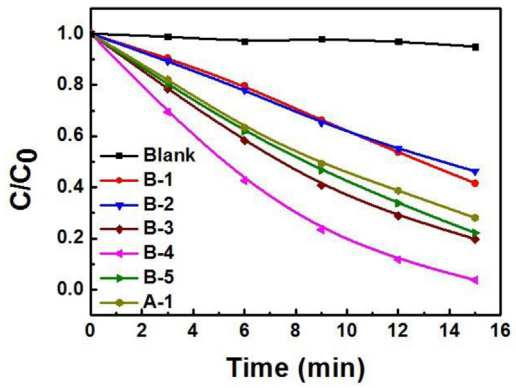

Fig. 5. The photodegradation of RhB with different photocatalyst Bi_2MoO_6 (B-1), 2 wt% Ag/AgCl-Bi_2MoO_6 (B-2), 10 wt% Ag/AgCl-Bi_2MoO_6 (B-3), 20 wt% Ag/AgCl-Bi_2MoO_6 (B-4), 30 wt% Ag/AgCl-Bi_2MoO_6 (B-5) and Ag/AgCl (A-1) under visible-light irradiation.

further investigated by HRTEM. The HRTEM images in Fig. 2c and d present the lattice spacings determined to be 0.276, 0.167 and 0.102 nm, which are indexed to the d spacings of the Bi_2MoO_6 (0 0 2) plane [35], AgCl (3 1 1) plane, and Ag (4 0 0) plane, respectively. The HRTEM result further confirms that the surfaces of the Bi_2MoO_6 nanospheres are decorated by the Ag/AgCl nanoparticles. The formation of Ag/AgCl-Bi_2MoO_6 microstructure can fully use the outer surfaces of Ag/AgCl and interfaces between Ag/AgCl and Bi_2MoO_6, which may improve the separation efficiency of charge carriers and photocatalytic activity of the composite.

The UV–vis diffuse-reflectance spectra of Bi_2MoO_6 and Ag/AgCl-Bi_2MoO_6 are illustrated in Fig. 3. The pure Bi_2MoO_6 presents absorption from the UV through the visible range up to 490 nm, which could be responsible for the visible light catalytic activity. After introducing Ag/AgCl species, the Ag/AgCl-Bi_2MoO_6 sample shows clearly enhanced absorption in the visible light range with a wide absorption range around 490–570 nm. It is obvious that the presence of Ag/AgCl enhances the absorption ability of the photocatalyst in the visible-light region, which is mainly due to the surface plasmon absorption of sliver [36] and interaction between Ag and AgCl. It should be beneficial to the catalytic activity of Bi_2MoO_6 sample. The phenomenon is also certificates that Ag/AgCl-Bi_2MoO_6 sample contains Ag nanoparticles, which are photo-reduced from AgCl.

The elemental composition and chemical status of the as-prepared samples were examined by X-ray photoelectron spectroscopy (XPS). Fig. 4a–e shows the XPS spectra of the Ag/AgCl-Bi_2MoO_6 sample. The survey spectrum in Fig. 4a demonstrates that the main elements in the sample are Bi, Mo, O, Ag, Cl and C. Fig. 4b shows Bi 4f XPS spectrum of sample Ag/AgCl-Bi_2MoO_6, two peaks are observed at approximately 159.2 eV and 164.5 eV, which are ascribed to the Bi $4f_{7/2}$ and Bi $4f_{5/2}$ binding energies, respectively. Fig. 4c gives the binding energies of Mo $3d_{5/2}$ and Mo $3d_{3/2}$ peaks in the samples, which are located at 232.4 and 235.4 eV, respectively [37]. Fig. 4d presents Ag 3d XPS spectrum of Ag/AgCl-Bi_2MoO_6 sample, two peaks are observed at approximately 367.1 eV and 373.1 eV, which are ascribed to the Ag $3d_{5/2}$ and Ag $3d_{3/2}$ binding energies, respectively. Each of the peaks could be further deconvoluted into two peaks, at about 367.1/368.2 eV and 373.1/374.2 eV, respectively. The peaks at 367.1 eV and 373.1 eV can be attributed to Ag^+, whereas the peaks at 368.2 eV and 374.2 eV can be ascribed to Ag^0, similar results have also been reported by other groups [17,38,39]. The Cl 2p spectrum (Fig. 4e) of the Ag/AgCl-Bi_2MoO_6 sample shows that the binding energies of Cl $2p_{3/2}$ and $2p_{1/2}$ are approximately 198.0 eV and 199.8 eV, respectively. The XPS results confirm the existence of Ag^0 in the sample Ag/AgCl-Bi_2MoO_6, which consistent with the XRD results (Fig. 1).

3.2. Visible-light photocatalytic activity of Ag/AgCl-Bi_2MoO_6 samples

The photocatalytic activity of the Bi_2MoO_6, Ag/AgCl-Bi_2MoO_6 and Ag/AgCl samples was evaluated by the degradation of organic dyes under visible light irradiation. Rhodamine B (RhB) was chosen as a representative hazardous dye to evaluate the photocatalytic performance. The photo-degradation process of RhB was recorded by the temporal evolution of the UV–vis absorption spectrum and all the samples were processed in the same procedure. Fig. 5 shows that the degradation curves of RhB over Bi_2MoO_6,

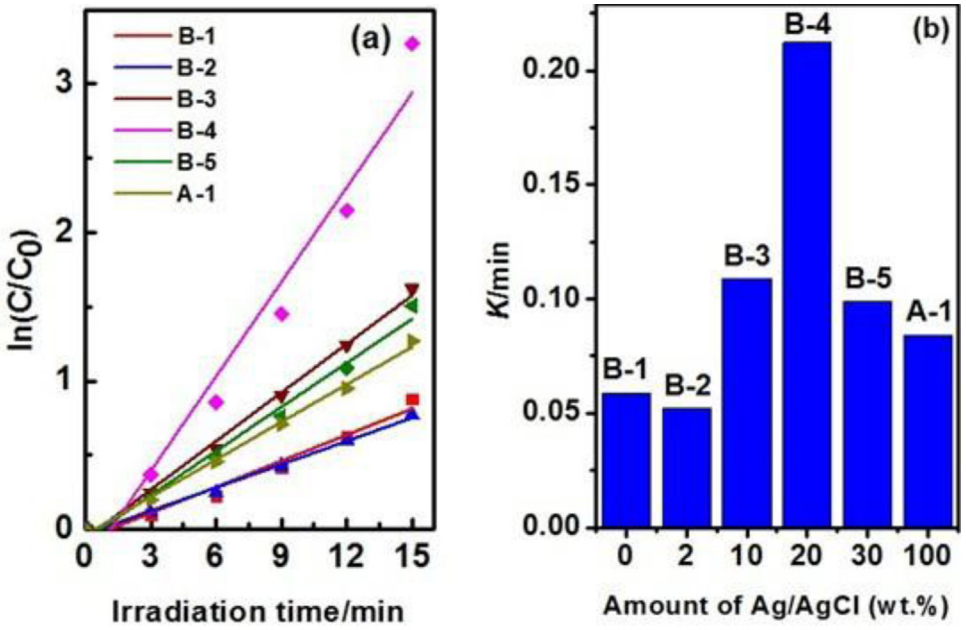

Fig. 6. (a) The first-order kinetics of RhB degradation in the presence of Ag/AgCl-Bi_2MoO_6 photocatalysts with different Ag/AgCl content: 0 wt% (B-1), 2 wt% (B-2), 10 wt% (B-3), 20 wt% (B-4), 30 wt% (B-5) and 100 wt% (A-1). (b) The degradation rate constant of RhB with different samples.

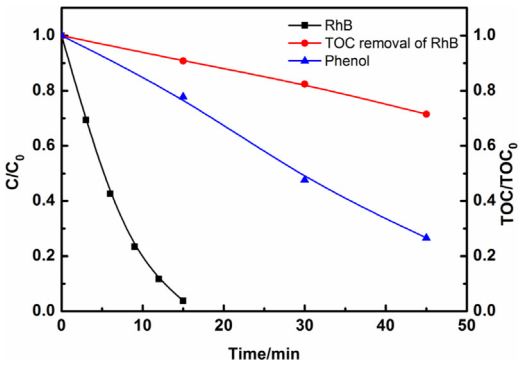

Fig. 7. The photodegradation (black line) and TOC removal (red line) curves of RhB dye, and the phenol photo-decomposition curve (blue line) over 20 wt% Ag/AgCl-Bi_2MoO_6 sample under visible irradiation. (For interpretation of the references to color in this figure legend as well as in the text, the reader is referred to the web version of this article.)

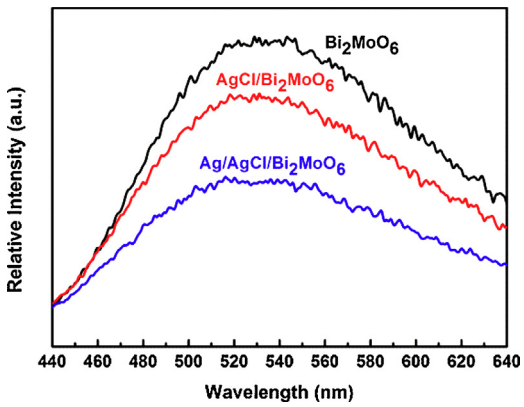

Fig. 9. Photoluminescence spectra (PL) of the Bi_2MoO_6, 20 wt% AgCl/Bi_2MoO_6 and 20 wt% Ag/AgCl-Bi_2MoO_6 photocatalysts.

Ag/AgCl-Bi_2MoO_6 and Ag/AgCl photocatalysts as a function of irradiation time are plotted at a certain time interval. The blank experiment indicates that the degradation of RhB can be negligible in the absence of photocatalyst. The photocatalytic activity of the Ag/AgCl-Bi_2MoO_6 sample increases with the increasing Ag/AgCl content, and the 20 wt% Ag/AgCl-Bi_2MoO_6 shows the highest degradation efficiency (B-4). When the Ag/AgCl content is higher than 20 wt%; the photoactivity of the Ag/AgCl-Bi_2MoO_6 sample decreases. It may be attributed to reason that the larger Ag/AgCl nanoparticle size lead to the anchored force between the substrate and Ag/AgCl becomes weaker, which could destruct the heterojunction structure, and lead to decreasing of photoactivity. The corresponding $\ln(C/C_0)$ plot has a good linearity (Fig. 6a), indicating that the sunlight-driven photodegradation of RhB solutions in the presence of Ag/AgCl-Bi_2MoO_6 follows the first order kinetics. The degradation rate constant of RhB is shown in Fig. 6b. The degradation rate constant of 20 wt% Ag/AgCl-Bi_2MoO_6 is about 4 times to the pure Bi_2MoO_6. The result confirms that the synergetic effect between the Ag/AgCl and Bi_2MoO_6 is beneficial to the improvement of catalytic activity.

In the process of photocatalysis, it is important to evaluate the mineralization ability of catalysts. The degradation and TOC removal rate of RhB dye in the photocatalytic process are depicted in Fig. 7. Obviously, the rate of TOC reduction (red line) was much slower than the photodegradation of RhB dye (black line). The decoloration of RhB dye reached to 100% after 15 min visible irradiation, however, only ten percent of mineralized degree was achieved. After 45 min irradiation, about 30% of organic carbon was removed from the solution, which suggested that the RhB was easy to mineralize. Furthermore, the flower-like Ag/AgCl-Bi_2MoO_6 photocatalyst can be used to degrade the other colorless organics, such as phenol. As shown in Fig. 7 (blue line), photodegradation of phenol reached to 75% after 45 min visible irradiation. The results indicate that the flower-like Ag/AgCl-Bi_2MoO_6 composite photocatalyst can also has high performance in catalyzing degradation of colorless organics.

The stability of photocatalyst is one of the most important parts for its practical application; the cycling experiment was investigated with the B4 sample (20 wt% Ag/AgCl-Bi_2MoO_6). The sample was recycled by centrifugation and then washed with water in the experiments. As shown in Fig. 8, the photocatalytic efficiency of B-4 sample presents a slightly loss in recycle experiment. The slightly decrease in catalytic activity may be attributed to the little loss of the catalyst in the cycling experiment. Therefore, the Ag/AgCl-Bi_2MoO_6 composite can be regarded as stable photocatalysts under visible light irradiation.

3.3. Photocataytic mechanism discussion

To verify the photocatalytic mechanism, the PL, SPV and ESR techniques were performed. The electron–hole separation efficiency of photocatalyst is a very important factor of the photocatalytic activity. PL spectra reveal the migration, transfer, and recombination processes of the photogenerated electron–hole pairs in semiconductors. The PL emission spectrum of the samples was measured with excitation light of $\lambda = 395$ nm; and the results are shown in Fig. 9. It clearly indicates that Bi_2MoO_6 shows an emission peak centered at around 535 nm. The PL emission intensities of the samples decreased after the introducing of AgCl and Ag/AgCl

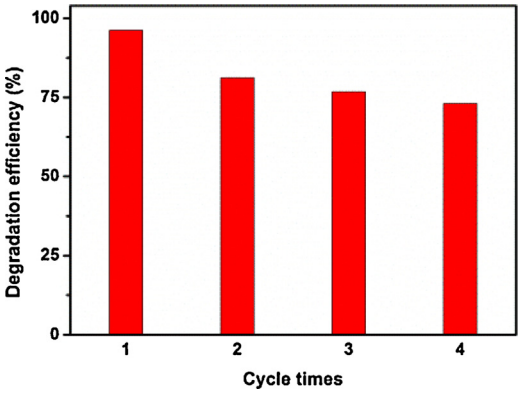

Fig. 8. Cycling runs for the photocatalytic RhB degradation in the presence of 20 wt% Ag/AgCl-Bi_2MoO_6 photocatalyst.

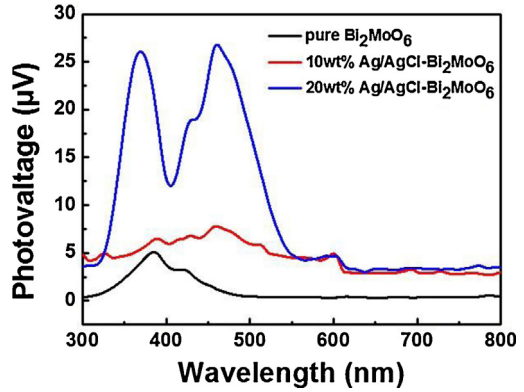

Fig. 10. SPV spectra of the pure Bi_2MoO_6, 10 wt% Ag/AgCl-Bi_2MoO_6 and 20 wt% Ag/AgCl-Bi_2MoO_6.

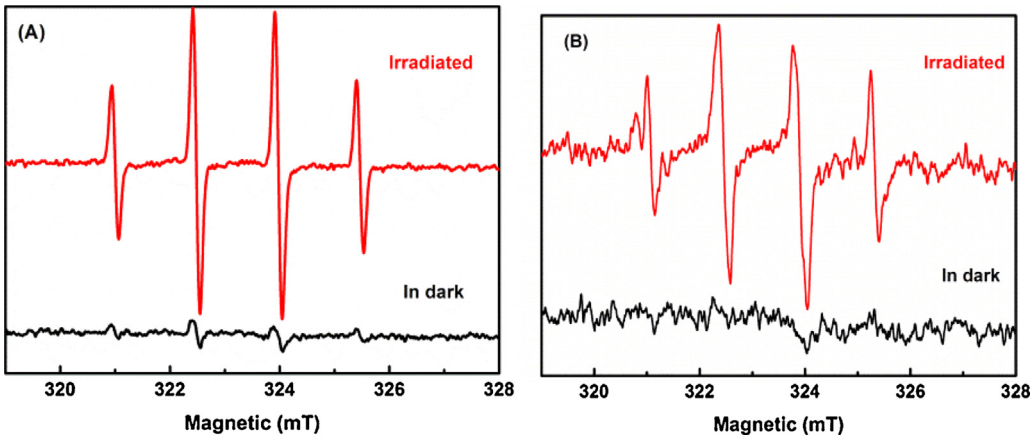

Fig. 11. ESR spectra record at ambient temperature with 20 wt% Ag/AgCl Bi_2MoO_6 photocatalyst in: (A) H_2O (B) DMSO.

species. The decreasing emission intensity of Ag/AgCl-Bi_2MoO_6 sample suggests the recombination of charge carriers is hindered effectively, and it may be beneficial to improve the photocatalytic ability.

In order to further investigate the photocatalytic mechanism, surface photovoltage spectroscopy (SPV) is conducted, which reveals the dynamic behaviors of the photogenerated charges in the Ag/AgCl-Bi_2MoO_6 samples [40]. Fig. 10 gives the SPV spectra of pure Bi_2MoO_6, 10 wt% Ag/AgCl-Bi_2MoO_6 and 20 wt% Ag/AgCl-Bi_2MoO_6 samples. The pure Bi_2MoO_6 presents an apparent SPV response range from 300 to 500 nm. Furthermore, with the Ag/AgCl coupling, the SPV response region of Ag/AgCl-Bi_2MoO_6 composite is broaden, which indicates that the photogenerated electron–hole pairs separated more effectively. The SPV response intensity of the Ag/AgCl-Bi_2MoO_6 sample increases with the increasing Ag/AgCl content, and the 20 wt% Ag/AgCl-Bi_2MoO_6 shows the highest SPV response intensity. The increased SPV intensity indicates that introducing an appropriate amount of Ag/AgCl is beneficial for the separation of photogenerated electron–hole pairs in Bi_2MoO_6.

The ESR spin-trap technique with 5,5-dimethyl-1-pyrrolineN-oxide (DMPO) was further employed to probe the nature of the reactive oxygen species generated on the surface of the catalysts under visible light irradiation. Fig. 11 shows ESR spectra measured as the effect of light irradiation on the 20 wt% Ag/AgCl-Bi_2MoO_6 photocatalyst at room temperature in air. There is no ESR signal in the dark, however, the significant evolution of ESR signals in H_2O and DMSO system can be observed under visible light irradiation. Four characteristic peaks of DMPO-•OH (with a 1:2:2:1 intensity ratio, red line, Fig. 11A, B) in both H_2O and DMSO system are observed in the ESR spectrum of the Ag/AgCl/Bi_2MoO_6 suspension, which is consistent with the similar spectra reported by other groups for the DMPO-•OH adducts [41,42]. However, no such signals were detected in the dark, which means that visible light irradiation is essential for the generation of •OH on the surface of the catalyst. These active species will result in the degradation of RhB in the Ag/AgCl-Bi_2MoO_6 sample.

Based on the above results and analysis, a possible mechanism for the photocatalytic activity enhancement of the Ag/AgCl-Bi_2MoO_6 nanostructure is proposed (as shown in Fig. 12). From the image shown in Fig. 12(a) Ag nanoparticles can absorb the visible light and generate electron–hole pairs due to SPR effect. With visible light irradiation, photogenerated electron–hole pairs are separated on the surface of Ag NPs. The SPR excited hot electrons have energy between 1.0 and 4.0 eV with respect to the metal Fermi level [32]. Therefore, the excited electrons have enough energy to transfer from Ag NPs to conduction band (CB) of AgCl and Bi_2MoO_6. At the same time, in Fig. 12(b) the Bi_2MoO_6 can be excited by the visible-light, the electron–hole pairs generate under the visible light irradiation. Subsequently, the electrons in AgCl and Bi_2MoO_6 will be trapped by absorbed O_2 and H_2O to form •OH. The holes

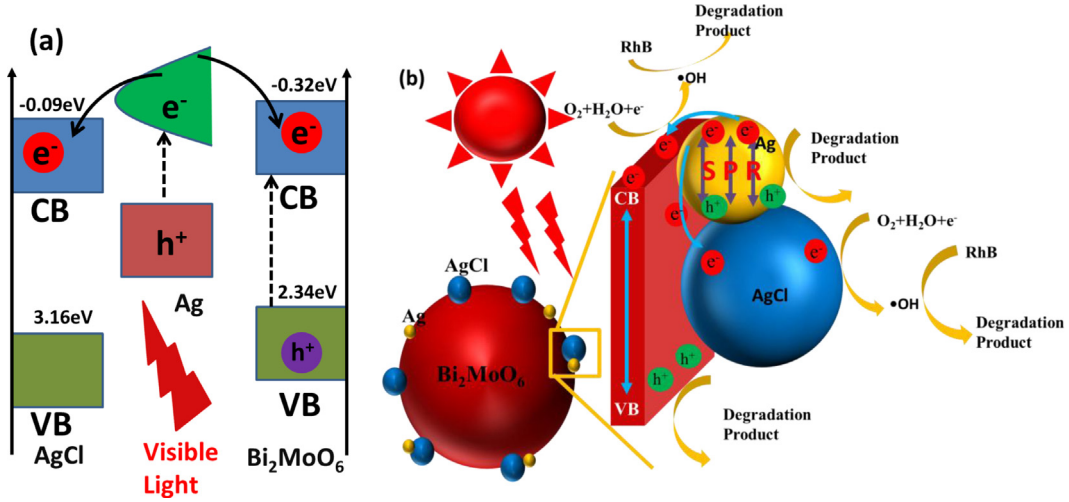

Fig. 12. (a) Ag nanoparticles can absorb the visible light and generate electron–hole pairs due to SPR effect. (b) Schematic diagram illustrating the proposed degradation mechanism of organic pollutants over Ag/AgCl-Bi_2MoO_6 samples.

accumulated on Bi_2MoO_6 and Ag NPs surface can oxidize organic pollutants. Therefore, the Ag/AgCl-Bi_2MoO_6 samples exhibit superior activity for decomposition of organic pollutants.

4. Conclusions

In summary, an Ag/AgCl-Bi_2MoO_6 composite was prepared by using flower-like Bi_2MoO_6 spheres as a support, through the deposition of AgCl nanoparticles on the surface of Bi_2MoO_6 spheres. The as-prepared Ag/AgCl-Bi_2MoO_6 composite showed a greatly enhanced visible-light photocatalytic activity for degradation of RhB compared to those of pure Bi_2MoO_6 and Ag/AgCl. The experiment results showed that the 20 wt% Ag/AgCl-Bi_2MoO_6 had the highest photoactivity. The Ag/AgCl anchored on the surface of the Bi_2MoO_6 could transfer the charge carriers generated from Bi_2MoO_6 and suppress the electron–hole recombination. The PL, SPV and ESR experiment illustrated that the synergistic effect between Ag/AgCl and Bi_2MoO_6 was very important to the enhancement of the photoactivity of Ag/AgCl-Bi_2MoO_6. This work provides a facile way to achieve highly efficient photocatalysts, which could be used to develop hybrid composite with promising applications in water pollution purification.

Acknowledgements

This work was financially supported by the National Science Foundation of China (Grant No. 21003157 and 21273285), Beijing Nova Program (Grant No. 2008B76), and Science Foundation of China University of Petroleum, Beijing (Grant No. KYJJ2012-06-20).

References

[1] A. Fujishima, K. Honda, Nature 238 (1972) 37–38.
[2] C.C. Chen, W.H. Ma, J.C. Zhao, Chem. Soc. Rev. 39 (2010) 4206–4219.
[3] D.Q. Zhang, G.S. Li, J.C. Yu, J. Mater. Chem. 20 (2010) 4529–4536.
[4] G. Liu, Y.N. Zhao, C.H. Sun, F. Li, G.Q. Lu, H.M. Cheng, Angew. Chem. Int. Ed. 47 (2008) 4516–4520.
[5] J.L. Zhang, Y.M. Wu, M.Y. Xing, S.A.K. Leghari, S. Sajjad, Energ. Environ. Sci. 3 (2010) 715–726.
[6] X.B. Chen, S.H. Shen, L.J. Guo, S.S. Mao, Chem. Rev. 110 (2010) 6503–6570.
[7] M.R. Hoffmann, S.T. Martin, W.Y. Choi, D.W. Bahnemann, Chem. Rev. 95 (1995) 69–96.
[8] S.T. Kochuveedu, D.P. Kim, D.H. Kim, J. Phys. Chem. C 116 (2012) 2500–2506.
[9] X.B. Chen, L. Liu, P.L. Yu, S.S. Mao, Science 331 (2011) 746–750.
[10] F. Zuo, L. Wang, T. Wu, Z.Y. Zhang, D. Borchardt, P.Y. Feng, J. Am. Chem. Soc. 132 (2010) 11856–11857.
[11] G.H. Tian, Y.J. Chen, W. Zhou, K. Pan, Y.Z. Dong, C.G. Tian, H.G. Fu, J. Mater. Chem. 21 (2011) 887–892.
[12] Q.J. Ruan, W.D. Zhang, J. Phys. Chem. C 113 (2009) 4168–4173.
[13] X. Xiao, W.D. Zhang, J. Mater. Chem. 20 (2010) 5866–5870.
[14] L.W. Zhang, Y. Man, Y.F. Zhu, ACS Catal. 1 (2011) 841–848.
[15] Y.S. Xun, W.D. Zhang, Dalton Trans. 42 (2013) 1094–1101.
[16] G.H. Tian, Y.J. Chen, X.Y. Meng, J. Zhou, W. Zhou, K. Pan, C.G. Tian, Z.Y. Ren, H.G. Fu, ChemPlusChem 78 (2013) 117–123.
[17] Y.G. Xu, H. Xu, J. Yan, H.M. Li, L.Y. Huang, J.X. Xia, S. Yin, H.M. Shu, Colloid Surf. A 436 (2013) 474–483.
[18] D. Chen, J.H. Ye, Adv. Funct. Mater. 18 (2008) 1922–1928.
[19] C.M.C. Vera, R. Aragon, J. Solid. State. Chem. 181 (2008) 1075–1079.
[20] Y. Shimodaira, H. Kato, H. Kobayashi, A. Kudo, J. Phys. Chem. B 110 (17) (2006) 790–17797.
[21] H.H. Li, C.Y. Liu, K.W. Li, H. Wang, J. Mater. Sci. 43 (2008) 7026–7043.
[22] L. Kong, Z. Jiang, T.C. Xiao, L.F. Lu, M.O. Jones, P.P. Edwards, Chem. Commun. 47 (2011) 5512–5514.
[23] H.F. Cheng, B.B. Huang, Y. Dai, X.Y. Qin, X.Y. Zhang, Langmuir 26 (2010) 6618–6624.
[24] A. Pearson, S.K. Bhargave, V. Bansal, Langmuir 27 (2011) 9245–9252.
[25] M.C. Long, W.M. Cai, J. Cai, B.X. Zhou, X.Y. Chai, Y.H. Wu, J. Phys. Chem. B 110 (2006) 20211–20216.
[26] L. Ge, C.C. Han, J. Liu. Appl. Catal. B: Environ. 108–109 (2011) 100–107.
[27] M.Y. Zhang, C.L. Shao, J.B. Mu, Z.Y. Zhang, Z.C. Guo, P. Zhang, Y.C. Liu, CrystEngComm 14 (2012) 605–612.
[28] Y.G. Xu, H. Xu, H.M. Li, J.X. Xia, C.T. Liu, L. Liu, J. Alloys Compd. 509 (2011) 3286–3292.
[29] J.F. Guo, B.W. Ma, A.Y. Yin, K.N. Fan, W.L. Dai, Appl. Catal. B: Environ. 101 (2011) 580–586.
[30] H. Cheng, B. Huang, P. Wang, Z. Wang, Z. Lou, J. Wang, X. Qin, X. Zhang, Y. Dai, Chem. Commun. 47 (2011) 7054–7056.
[31] K. Fuku, R. Hayashi, S. Takakura, T. Kamegawa, K. Mori, H. Yamashita, Angew. Chem. Int. Ed. 52 (2013) 7446–7450.
[32] S. Linic, P. Christopher, D.B. Ingram, Nat. Mater. 10 (2011) 911–921.
[33] V.G. Plotnichenko, D.V. Philippovskiy, V.O. Sokolov, V.F. Golovanov, G.V. Polyakova, L.S. Lisitsky, E.M. Dianov, Opt. Lett. 38 (2013) 2965–2968.
[34] Y.G. Sun, Nanoscale 2 (2010) 1626–1642.
[35] L.W. Zhang, T.G. Xu, X. Zhao, Y.F. Zhu, Appl. Catal. B: Environ. 98 (2010) 138–146.
[36] Y. Wang, Y.Q. Zheng, C.Z. Huang, Y.N. Xia, J. Am. Chem. Soc. 135 (2013) 1941–1951.
[37] Y.J. Chen, G.H. Tian, Y.H. Shi, Y.T. Xiao, H.G. Fu, Appl. Catal. B: Environ. 164 (2015) 40–47.
[38] M.S. Zhu, P.L. Chen, M.H. Liu, ACS Nano 5 (2011) 4529–4536.
[39] M.S. Zhu, P.L. Che, M.H. Liu, Langmuir 28 (2012) 3385–3390.
[40] J. Su, X.X. Zou, G.D. Li, X. Wei, C. Yan, Y.N. Wang, J. Zhao, L.J. Zhou, J.S. Chen, J. Phys. Chem. C 115 (2011) 8064–8071.
[41] X.F. Zhou, C. Hu, X.X. Hu, T.W. Peng, J.H. Qu, J. Phys. Chem. C 114 (2010) 2746–2750.
[42] X.J. Bai, L. Wang, R.L. Zong, Y.F. Zhu, J. Phys. Chem. C 117 (2013) 9952–9961.